



Contents lists available at ScienceDirect

Catalysis Today

journal homepage: www.elsevier.com/locate/cattod

Green fabrication of 2D platinum superstructures and their high catalytic activity for mitigation of organic pollutants

N.K.R. Bogireddy^a, U. Pal^b, M.K. Kumar^c, J.M. Domínguez^d, L. Martinez Gomez^c, V. Agarwal^{a,*}

^a Centro de Investigación en Ingeniería y Ciencias Aplicadas, UAEM, Av. Univ. 1001, Col. Chamilpa, Cuernavaca, Morelos, 62209, Mexico

^b Instituto de Física, Benemérita Universidad Autónoma de Puebla, Apdo. Postal J-48, Puebla Pue., 72570, Mexico

^c Universidad Nacional Autónoma de México, Instituto de Ciencias Físicas, Avenida Universidad s/n, Cuernavaca, MOR, 62210, Mexico

^d Instituto Mexicano del Petróleo, Eje Central L. Cárdenas Norte 152, 07730, San Bartolo Atepehuacan, Gustavo A. Madero, México City, Mexico

ARTICLE INFO

Keywords:

Self-assembly
Platinum
Nanoparticles
Catalytic reduction
4-Nitrophenol
Methylene blue

ABSTRACT

We report a simple eco-friendly green synthesis of self-assembled (SA) Pt nanoparticles, forming 2D sub-micrometric structures, from *Coffea Arabica* seed (CAS) extract. Small (~2 nm) spherical Pt nanoparticles organized in the form of square/rectangular shaped 2D superstructures, have been utilized as efficient reusable catalysts for the reduction of industrial pollutants such as 4-nitrophenol (4-NP), methylene blue (MB) and their mixtures in aqueous medium (as well as in adsorbed state), with the activity parameters 0.75, 0.68 and 0.94 s⁻¹ mg⁻¹, respectively. The green process utilized for the fabrication of platinum superstructures in the present work could be extended for the fabrication of other metallic superstructures for efficient reusable catalytic reduction of organic contaminants.

1. Introduction

Self-assembled (SA) metal nanoparticles with unique optical and detection/sensing functionalities, have been used for electronics, biomedicine and catalysis [1–4]. Although, it is challenging to develop simple and sustainable approaches for the synthesis of SA nanostructures, some groups have demonstrated the fabrication of two-dimensional (2D)/ three-dimensional (3D) superstructures [5], such as nanowires/tubes [6], nano-rods [7] and core-shell structures [8]. While the nanoparticles of Pt and their bimetallic alloys, supported on carbon nanotubes and metal oxides (SiO₂, TiO₂ and Al₂O₃), have been utilized successfully in catalysis, batteries, fuel cells and gas diffusion electrodes [9,10], chemically synthesized self-assembled Pt nanostructures (nanocube, cuboctahedral, octahedral), have been tested as efficient electro-catalysts for the oxidation of methanol and ethanol [9], adsorption and desorption of hydrogen, hydrogenation of ethylene, benzene and p-nitrophenol [11–20].

In general, chemical synthesis routes use toxic chemicals and high temperatures [21–23], so the efforts have been devoted to develop novel, cost effective, simple and biocompatible methods for the synthesis of self-assembled and reusable platinum nanoparticles. Although Yongsoon et al., [24], reported the green synthesis and characterization of self-assembled Pt nanoparticles to form nanowires in an aqueous glucose solution at pH 8.0 using hydrothermal treatment at

100 °C, they weren't demonstrated for any possible catalytic application. On the other hand, Stefanos et al., [25] reported the chemical synthesis of hydrophilic Pt nanoflowers for their application as reusable catalyst and the performance was verified towards the reduction of 4-NP. Qianli et al., [26], fabricated an ordered mesoporous CeO₂-supported reusable Pt nanocatalyst and demonstrated its efficiency for the reduction of 4-NP. Jyun-Guo et al., [27], synthesized poly(diallyldimethylammonium chloride) [PDDA]-stabilized platinum nanoparticles (NPs) for the efficient reduction of 4-NP. Yunus et al. [28], reported highly efficient and reusable Pt/Rh nanoparticles confined in Graphene Oxide layered structures for methylene blue removal from aqueous solutions. Hakan et al., [29], fabricated reusable activated carbon furnished monodisperse Pt nanocomposites as adsorbent for methylene blue removal from aqueous solutions. Lingyun et al. [30], reported the use of monodisperse CuFe₂O₄ nanoparticles for the selective degradation of methylene blue from mixed aqueous solutions of organic dyes. Yang et al., [31] reported modular polyoxometalate-layered double hydroxide composites for the catalytic degradation of a mixture of rhodamine B, methylene blue and crystal violet.

In the present work, we demonstrate a simple, sustainable, and green approach for the synthesis of monodispersed Pt nanoparticles and their self-assembly using *Coffea Arabica* seed (CAS) extract both reducing and stabilizing agent. The oxidized protocatechuic acid (quinone) groups of CAS extract work as effective ligand for the self-assembly of

* Corresponding author.

E-mail address: vagarwal@uaem.mx (V. Agarwal).

<https://doi.org/10.1016/j.cattod.2019.06.044>

Received 4 February 2019; Received in revised form 28 May 2019; Accepted 13 June 2019

0920-5861/ © 2019 Elsevier B.V. All rights reserved.

monodispersed Pt nanoparticles. The non-covalent interactions between the organic-inorganic moieties along with cooperative hydrogen bonds between the macrocycles not only provide the required stability to the formed Pt nanoparticles, but also help them to assemble in two-dimensional super-structures. The square and rectangular shaped stable 2D superstructures have been tested for the degradation of organic pollutants such as 4-nitrophenol (4-NP), methylene blue (MB) and their mixtures, both in their aqueous solution and in adsorbed state. The catalytic efficiency of the proposed self-assembled structure has been found to be higher than the already reported reusable catalysts.

2. Materials and methods

2.1. Materials

Chloro-platinic acid ($\text{H}_2\text{PtCl}_6 \cdot \text{H}_2\text{O}$, Sigma Aldrich, 99.9%), 4-nitrophenol (4-NP, Sigma Aldrich, 99.5%), Methylene blue (MB, 99%), sodium borohydride (NaBH_4 , Sigma Aldrich, 98%), silica (Sigma Aldrich, 99.9%) and all other reagents were of analytical grade, and utilized as received. Green *Coffea Arabica* Seeds (CAS) were collected from the local market of Cuernavaca city, Morelos state, Mexico. Double distilled (DD) water was utilized throughout during the synthesis process.

2.2. Preparation of CAS extract

CAS, collected from the local market, were dried, grinded to fine powder, and stored in ambient conditions. For the preparation of CAS extract, 0.6 g of finely ground CAS powder was mixed with 50 mL of DD water and kept at $\approx 85^\circ\text{C}$ for 35 min. The extract was filtered using a $0.2\ \mu\text{m}$ cellulose nitrate filter paper (CNFP). The natural pH of the obtained CAS extract was found to be ≈ 6 .

2.3. Preparation of self-assembled platinum superstructures

An aqueous platinum ion solution ($0.01\ \text{M}\ \text{H}_2\text{PtCl}_6$) was added to 25 mL of boiling CAS extract in 1:5 volumetric ratio under constant magnetic stirring. In about 30 min, the color of the solution changed from brown to black, indicating the reduction of Pt ions and formation of Pt nano-/microstructures. The formed Pt nano-/microstructures were separated and washed 2–3 times by centrifugation and re-dispersed in DD water for their characterization.

The formation of Pt nanoparticles from stepwise reduction of the platinum salt (H_2PtCl_6) by CAS extract can be represented as follows:



2.4. Characterization

UV-vis optical absorption spectra of the colloidal structures ($100\ \mu\text{L}$ of SA-PtNPs in 2 mL of DD water) along with the CAS extract ($0.06\ \text{g}/10\ \text{mL}$) and platinum ion ($1\ \text{mM}$) solution were recorded using Perkin-Elmer Lambda 950 UV-vis dual beam spectrophotometer. A JEOL JEM 2100 transmission electron microscope (TEM) operating at 200 kV accelerating voltage and a Hitachi SU5000 Schottky field emission scanning electron microscope (FESEM) operating at 20 kV, were utilized to study the morphology, size, and elemental composition of the fabricated superstructures. For TEM and FESEM analysis, the diluted (1000 times) sample was sonicated for 1 h before drop casting onto a Cu grid and aluminum sample holder for TEM and FESEM analysis, respectively. X-ray diffraction (XRD) pattern of the fabricated structures (as-prepared SA-PtNPs powder) was recorded in a Bruker D8 Advance eco diffractometer after drying them at room temperature. A Varian 660 Fourier transform infrared (FT-IR) spectrophotometer with ATR accessory was utilized to investigate the constituents of CAS powder and the

functional groups at the surface of fabricated platinum superstructures (in powder form). Dynamic light scattering (Malvern zetasizer, Model nano ZS) technique was used to determine the average size and size distribution of the fabricated superstructures. The DLS measurements were performed using 100 times diluted as-prepared SA-PtNPs. UV-vis absorption spectroscopy was additionally utilized to verify the proposed formation mechanism and to study the effect of solution pH on the disassembly/defragmentation of the self-assembled superstructures.

2.5. Catalytic conversion of industrial organic pollutants

Catalytic activity of the fabricated Pt superstructures (self-assembled Pt nanoparticles, SA-PtNPs) in the degradation of industrial pollutants in aqueous systems, with NaBH_4 as reducing agent, was studied over typical organic pollutants 4-nitrophenol (4-NP) and methylene blue (MB), individually as well as in the mixture (4-NP + MB) form. Under the used experimental conditions, a complete reduction of the organic pollutants (4-NP and MB) was not observed by the simple addition of either NaBH_4 or SA-PtNPs individually.

For catalytic tests, $1\ \text{mM}$ aqueous solutions of 4-NP and MB were prepared by dissolving $0.278\ \text{mg}$ and $0.639\ \text{mg}$ of corresponding precursors in 2 mL of DD water, respectively. Then $0.76\ \text{mg}$ of NaBH_4 was added to 2 mL of the dye solution ($0.1\ \text{M}$). After about 10 min, $10\ \mu\text{L}$ of SA-PtNPs (stock solution with $8\ \text{mg}/\text{mL}$) was added to the mixture. Apart from the visual color change (from pale yellow to dark yellow, followed by a complete change to transparent solution) the degradation of 4-NP was followed by monitoring the intensities of the characteristic absorption bands associated to 4-NP (around $317\ \text{nm}$; color: pale yellow) and 4-nitrophenolate ions (around $400\ \text{nm}$; color: dark yellow). For MB, apart from the visual color change from blue to transparent, the decrement in the principal absorption bands located around 295 and $662\ \text{nm}$ were monitored.

To evaluate the catalytic efficiency of SA-PtNPs in the degradation of MB in adsorbed state, 2 mL of $1\ \text{mM}$ MB (same as the tests performed in liquid form) was adsorbed onto 30 mg of silica. For mixed NP and MB degradation in adsorbed form, the exactly same amount and concentration (as the liquid samples mentioned above) of NP and MB were drop-casted onto 30 mg of silica, and dried under ambient conditions.

The reusability of platinum superstructure (SA-PtNPs) catalysts in cationic dye degradation was tested by recovering them from the reaction mixtures through centrifugation at the end of each run, washing with ethanol (96%) and twice with DD water. The extracted SA-PtNPs were redispersed in DD water ($0.8\ \text{mg}/100\ \mu\text{L}$) and utilized in a fresh reaction solution. After each reaction cycle, the supernatant solution left after the extraction of the particles, was characterized to evaluate the degradation efficiency of the catalyst. The reusability tests were performed over 5 cycles.

3. Results and discussion

The reduction of Pt^{4+} ions by the boiling CAS extract and formation of Pt superstructures were initially monitored by recording the optical absorption spectra of as-prepared CAS extract, boiled CAS extract, and the colloidal solution of Pt structures after extracting them from the reaction solution. As can be seen in Fig. 1, the UV-vis absorption spectrum of as-prepared CAS extract has strong absorption in the UV region, with two clear absorption bands peaked around 273 and $320\ \text{nm}$. While the CAS extract revealed no absorption band after boiling, the Pt particles formed after the reduction of the Pt salt by CAS extract revealed two absorption bands peaked around 267 and $328\ \text{nm}$. It can be noticed further that the position of these absorption bands do not match with the absorption bands of the as-prepared CAS extract, indicating their distinct origin. As the colloidal Pt nanoparticles manifest broad absorption in the UV-vis spectral region with no distinct absorption peak in $250\text{--}500\ \text{nm}$ range [32,33], the absorption bands appeared in our CAS extract reduced Pt structures might be the result of

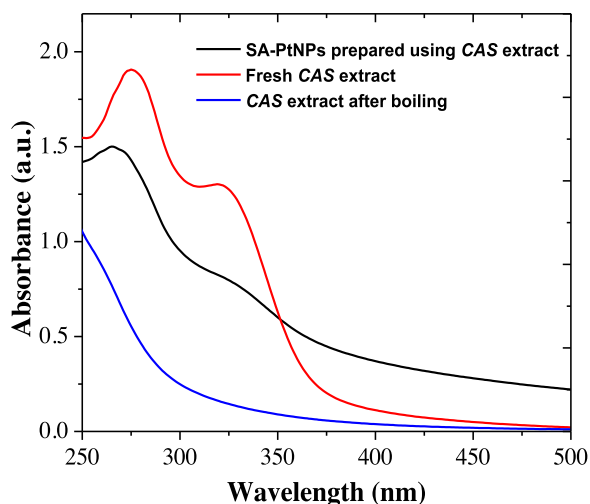


Fig. 1. UV–vis absorption spectra of freshly prepared filtered CAS extract, CAS extract after boiling (filtered) and the aqueous colloidal solution of SA-PtNPs (centrifuged and re-dispersed).

near field coupling between the surface plasmons of adjacent nanoparticles due to the transfer and confinement of electromagnetic energy as has been observed by Zhang et al. for PtNPs incorporated in photonic crystal made of spherical silica particles [34]. The strength of electromagnetic coupling in nanoparticle assembly is known to be controlled by the inter particle spacing and the dielectric constant of the medium. Additionally, the symmetry of nanoparticle arrays has been reported to determine the spatial distribution of charge polarizations and hence the splitting of plasmon bands of the assemblies [35].

As can be noticed from Fig. 2a, the XRD pattern of the fabricated Pt nano-/microstructures revealed several broad diffraction peaks at 40.8, 45.8, 67.1, 81.6 and 85.8° correspond to the (111), (200), (220), (311) and (222) planes of Pt in fcc phase (JCPDS file No. 04-0783), respectively. The sharp bands revealed around 28.5, 50.4, 58.9 and 73.8° correspond to graphitic carbon, probably appearing from the degradation of biomass contained in the CAS extract. Appearance of such sharp diffraction peaks associated to carbon in the XRD pattern has also been observed by Vardon et al. [36,37] for activated carbon and commercial Pt/C catalysts. As can be noticed, the diffraction peaks associated to Pt in the XRD pattern are broad, indicating the formation of small Pt particles. The average crystallite size (D) in the formed Pt submicron structures (revealed and explained as self-assembled PtNPs in the latter part of the discussion), calculated using (111) plane with Scherrer relation $D = 0.9\lambda/\beta\cos(\theta)$, was 2.0 ± 0.1 nm.

Self-assembly and the formation of macroscopic Pt superstructures in the sample can be clearly observed in the SEM image presented in Fig. 2b. Formation of 2D superstructures of square and rectangular shapes of 0.21–0.65 μm in length and 0.20–0.46 μm in width is very clear in the image. In order to identify the structural arrangement of the superstructures, they were analysed by TEM. Interestingly, TEM images (Fig. 2c) revealed the superstructures consist of very small spherical platinum nanoparticles of about 2 nm diameters (monodispersed PtNPs). Fig. S1 in electronic supporting information (ESI) shows the corresponding particle size distribution measured over 200 NPs from the HRTEM images (Fig. 2c). The HRTEM image and selected area electron diffraction (SAED) pattern (insets, Fig. 2c) of the PtNPs revealed their high crystallinity, with estimated inter planer spacing d of 0.225 nm, corresponding to (111) planes of Pt in fcc phase (JCPDS No. 04-0783). EDS spectra recorded on the Pt superstructures revealed only the Pt and C signals (Fig. 2f), confirming the presence of carbonaceous matter in the sub-micrometric Pt structures. In Fig. 2(d–f), typical secondary electron image (SEI) of a superstructure, along with Pt and C distributions (elemental mappings) over it are presented. As can be

seen, both Pt and C are uniformly distributed over the superstructures. The results indicate a direct contribution of the oxidized biomolecules of CAS extract in the formation of Pt superstructures through a possible intermolecular hydrogen bonding between each functionalized nanoparticle as illustrated in Fig. 3. In order to further confirm the absence of individual PtNPs in the sample and quantify the average dimensions of the self-assembled Pt superstructures, dynamic light scattering (DLS) technique was employed (Fig. S2 in ESI). The DLS spectrum presented in Fig. 2f clearly demonstrates the absence of individual PtNPs in the sample and formation of sub-micrometric superstructures with average hydrodynamic size of approx. 290 nm (Z-average). (A broad peak formed with an apparent combination of two peaks (when de-convoluted): one having a maximum at approx. 180 nm and the other at around 500 nm in close proximity with the width and length measured from the SEM images (Fig. 2b)).

For the fabrication of 2D platinum superstructures, we utilized an aqueous solution of CAS extract. The organic extract acted both as reductor of Pt^{4+} ions in the aqueous solution of H_2PtCl_6 and stabilizing agent for the formed PtNPs. As has been reported by Tang et al. [38,39], aqueous CAS extracts contain phytochemicals with one or more hydroxyl groups. Detailed possible formation mechanism for self-assembled platinum nanoparticles is presented in the supplementary information as Scheme S1 to S5.

A close proximity of such organic molecule-capped metal NPs results in the formation of well-defined organic-inorganic network or a lattice through intermolecular hydrogen bonding between the hydroxyl groups of the ester molecule and oxygen atoms of the quinones, as shown schematically in Fig. 3.

The above-mentioned hypothesis of self-assembled structures was verified via defragmentation performed as a function of pH. As the original pH of the CAS extract was ~ 6 , the centrifugation and re-suspension of the particles in DD water reveals a pH of around 6.5. Increasing the pH to more than 7.5 is found to defragment the sub-micron sized SA-PtNPs (absorption studies are given as Figure S3 in ESI).

To verify the mechanisms proposed for the formation and self-assembly of PtNPs, FTIR spectra of the freshly grinded CAS powder, (Fig. S4a; ESI) and the fabricated Pt superstructures (rinsed, filtered and dried) were recorded from 600 to 4000 cm^{-1} spectral range. As can be noticed, the FTIR spectrum of the as-prepared CAS powder revealed a broad absorption band in between 3000 and 3500 cm^{-1} , peaked around 3345 cm^{-1} , which can be attributed to the hydroxyl groups of polyphenolic compounds in CAS powder, forming part of the biomass around the PtNPs. The noticeable reduction in intensity of this band and its lower energy (3300 cm^{-1}) shift in the FTIR spectrum of Pt superstructures (Fig. S4b, ESI) indicate not only the presence of organic biomass around the formed PtNPs, but also the participation of protocatechuic acid in the reduction of Pt^{4+} ions and its subsequent oxidation.

The absorption bands at 2925 and 2851 cm^{-1} in the FTIR spectrum of CAS powder can be associated to the asymmetric and symmetric stretching vibrations of the C–H bond of protocatechuic acid and polyphenols, which reduced substantially after the reaction due to oxidation and esterification, respectively. A drastic reduction in intensity of the C–H stretching in the FTIR spectrum of the SA-PtNPs (Pt superstructures) clearly demonstrates the participation of protocatechuic acid in the reduction process of Pt^{4+} ions. The weak absorption band appeared around 2350 cm^{-1} both in FTIR spectrum of CAS extract and SA-PtNPs samples is associated to out of phase stretching vibration of $-\text{COO}-$.

The band appeared around 1701 cm^{-1} for the SA-PtNPs sample correspond to the C=O stretching vibration of 1, 2-benzoquinone moiety present in the oxidized protocatechuic acid. On the other hand, the absorption band appearing around 1558 cm^{-1} correspond to the out-of-phase stretching vibration of the carboxylate group of protocatechuic acid, bonded to the Pt NPs. The band at 1072 cm^{-1}

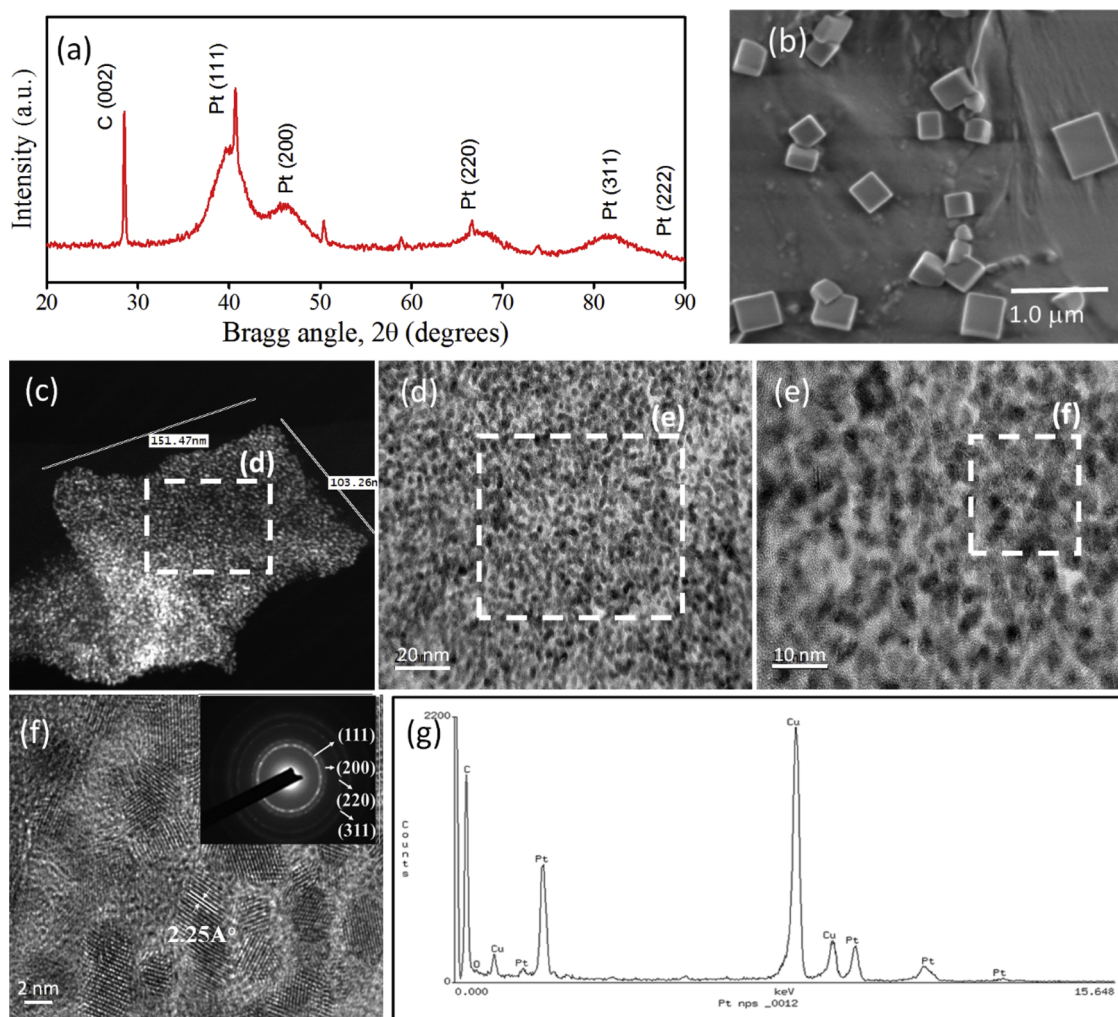


Fig. 2. (a) XRD spectrum, (b) typical SEM image, (c–f) typical TEM and HRTEM images of SA-PtNPs and (g) the EDS spectrum of SA-PtNPs revealing the presence of Pt ($M\alpha$) and Carbon ($K\alpha$). Presence of copper is seen due to the copper grid used to disperse the particles. A typical HRTEM image of constituting individual Pt NPs showing their crystalline lattice fringes, and corresponding selected area electron diffraction (SAED) pattern is shown as inset of (f).

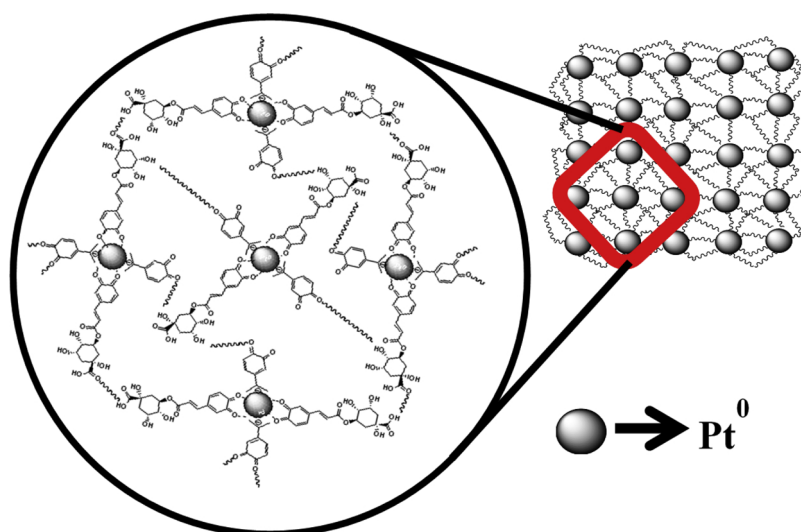


Fig. 3. Schematic presentation of the formation of organic-inorganic network (lattice) through intermolecular hydrogen bonding between the organic functional groups and the formation of 2D self-assembled Pt superstructures.

corresponds to the out of phase C–C–O stretching vibration in the polyol [40]. Finally, the appearance of absorption bands around 1240 and 750 cm^{-1} in the SA-PtNPs sample, which correspond to the C–O stretching vibration and the C–H wagging vibration in the aromatic ring of the phenol, clearly indicates the participation of phenolic compounds of CAS in the formation of Pt superstructures.

3.1. Catalytic degradation of industrial organic pollutants

Self-assembled nanostructures have shown fascinating prospects in the removal of organic pollutants from contaminated industrial air and water due to the ease of their reusability and enhanced efficiency [41–43]. In the present case, the Pt superstructures consisting biomass-capped small PtNPs provide high surface area, which facilitates the transportation of organic pollutant molecules and ions. The extensive surface area as well as the surrounding biomass of SA-PtNPs may additionally facilitates the adsorption and successively the reduction of industrial organic pollutants. Moreover, both electrostatic and π - π interaction between the biomass capped Pt superstructures and the dye molecules can be exploited to take full advantage of such materials in dye adsorption. As carbonaceous biomass can provide negative surface charges owing to deprotonation of oxygen containing functionalities, they are expected to reveal extraordinary adsorption capacity for cationic dyes. On the other hand, the unique morphology and macroscopic size of the superstructures offer additional advantages for pollutant separation and recycling. To verify the catalytic activity of the fabricated Pt superstructures in organic pollutant degradation, they have been tested for the degradation of 4-NP, MB, and 4-NP + MB mixtures in their aqueous solutions.

3.2. Catalytic degradation of 4-NP by Pt superstructures

Metal nanostructures are well-known catalysts for the degradation of pollutant organic molecules such as 4-NP. One of the limiting factors that determines their catalytic efficiency is the rapidity of charge exchange/transport, apart from their adsorption and reduction capacities. As the Pt superstructures fabricated in the present study contain carbonaceous biomass, they are expected to have a good charge transportation ability. On the other hand, due to their inherent structural configuration (consist of self-assembled Pt NPs of small sizes), they are expected to capture higher number of pollutant molecules at their surfaces.

An aqueous 4-NP solution of pale yellow color reveals a strong characteristic absorption band around 318 nm (Fig. 4a inset) in its UV–vis absorption spectrum. However, addition of NaBH_4 in this solution results in a visual color change (pale yellow to intense yellow) due to the formation of 4-nitrophenolate ion, with characteristic absorption band around 401 nm (Fig. 4a). After the addition of the catalyst (SA-PtNPs, 80 μg), the intensity of the absorption band decreased rapidly. Meanwhile, a new absorption band (peaked around 298 nm) appeared, indicating the formation of 4-AP (4-aminophenol) from 4-NP reduction [44,45]. The intensity of this (298 nm) absorption band increased with the increase of reaction time. The high reduction rate of 4-NP ion at the initial 60 s was probably due to the availability of active catalytic sites in high concentration at the initial stage. After initial adsorption/attachment of 4-NP ions, the number of free binding sites at the surface of the superstructures decreases, resulting in a slower reduction rate of 4-NP. Finally, the reaction stops with a visual color change from dark yellow to colorless within 240 s (photographic images of step by step reduction process are shown in Fig. S5 in ESI). The kinetics of the reduction reaction were analyzed using pseudo-first-order reaction, i.e., $\ln(C_t/C_0) = -kt$; where C_0 and C_t denote the initial concentration of organic pollutant and at time t , and k is the rate constant. As can be seen in Fig. 4d, the $\ln(C_t/C_0)$ vs t curve follows a linear relation with linear regression factor $R^2 = 0.996$. The first order reaction rate constant estimated from the slope of the linear fit was

$k = 6.0 \times 10^{-2} \text{ s}^{-1}$. Table 1 presents the comparison of the fabricated Pt superstructures with different types of Pt nanostructures and its composites as catalysts employed by different groups for the reduction of 4-NP.

Apart from that, calculated activity parameter, using the relation $k' = k/m$ (where m is the catalyst mass) was $0.75 \text{ s}^{-1} \text{ mg}^{-1}$, which is considerably higher than the reported activity parameters of nanostructured Pt thin film ($61.87 \times 10^{-2} \text{ s}^{-1} \text{ mg}^{-1}$) and pure bulk Pt ($3.22 \times 10^{-2} \text{ s}^{-1} \text{ mg}^{-1}$) [44,45]. The 4-NP reduction/degradation capacity (at time t) of the catalyst $Q_t = (A_0 - A_t) * M/m$ (where A_0 is the initial concentration and A_t is the final concentration of 4-NP at time t , m and M are the masses of catalyst and the organic pollutant solution, respectively) was calculated to be 17.37.

3.3. Catalytic reduction of methylene blue (MB) by Pt superstructures

The catalytic performance of SA-PtNPs was explored in the reduction of MB (0.278 mg) in the presence of NaBH_4 (0.76 mg) as a strong reducing agent utilized in the reduction of 4-NP as well. An aqueous MB solution shows absorption bands at 295 and 662 nm (Fig. 4b). With the addition of NaBH_4 , no visual change was observed in absorption spectrum or color of the MB solution. After the addition of catalyst (80 μg), the intensity of the absorption peaks corresponding to both the bands (295 and 662 nm) decreased rapidly. Within 60 s MB solution became colorless (photographic images shown in Fig. S5 in ESI), indicating its complete degradation and the formation of leuco MB (LMB) (Fig. 4b). The ultra-fast reduction of MB has been attributed to the presence of carbon in the catalyst (presence of carbon was confirmed by XRD, EDS and FTIR studies). The kinetics of MB reduction was analyzed using pseudo-first-order reaction ($R^2 = 0.993$; $k = 5.447 * 10^{-2} \text{ s}^{-1}$), obtaining an activity parameter ($k' = k/m$) of $0.68 \text{ s}^{-1} \text{ mg}^{-1}$. Similar to 4-NP, the reduction/degradation capacity (at time t) of MB was calculated from $Q_t = (A_0 - A_t) * M/m$ (A_0 and A_t being the initial and final concentrations (at time t) of MB; m and M are the masses of catalyst and the MB solution, respectively) to be 39.87. As can be observed in Table 2, the MB reduction activity of the Pt superstructures is substantially high in comparison to the MB reduction capacity of other Pt and non-Pt based catalysts reported in the literature.

3.4. Catalytic reduction of 4-NP + MB mixed pollutants

A 4-NP + MB mixture (0.135 mg of each in 1:1 proportion) was reduced by NaBH_4 (0.760 mg) in the presence of SA-PtNPs. Addition of NaBH_4 to the dye mixture results in a visual color change (photographic images are shown in Fig. S5 in ESI). The absorption spectrum of the mixture (4-NP + MB) solution revealed sharp absorption bands around 295, 401 and 661 nm (Fig. 4c) after the addition of NaBH_4 . Addition of the catalyst (80 μg) caused a significant intensity decrease for all three absorption peaks. As can be noticed, within 40 s (after catalyst addition), the 661 nm absorption band of MB disappeared completely, indicating a complete degradation of MB to LMB. However, the intensity of the 401 nm absorption band, which corresponds to 4-nitrophenolate ions, decreased close to zero in 300 s (the solution became colorless), with the positive evolution of a band corresponding to 4-AP at 298 nm (Fig. 4c). As can be noticed, it took a bit longer for the degradation of 4-NP in the 4-NP + MB mixture in comparison to its degradation in absence of MB. While the reaction in the present case also followed a pseudo-first-order reaction kinetics, estimated regression factor (R^2), reaction constant (k), and activity parameter (k') were $R^2 = 0.995$; $k = 7.57 * 10^{-2} \text{ s}^{-1}$ and $k' = 0.94 \text{ s}^{-1} \text{ mg}^{-1}$, respectively. The mechanisms involved in the reduction of organic pollutants are schematically depicted in Fig. 5.

The ultra-fast reduction observed both for MB and 4-NP is attributed to the high electrostatic interaction between negatively charged SA-PtNPs and positively charged MB/4-NP along with the π - π interaction induced adsorption of MB/4-NP on the SA-PtNPs micro-structures. As

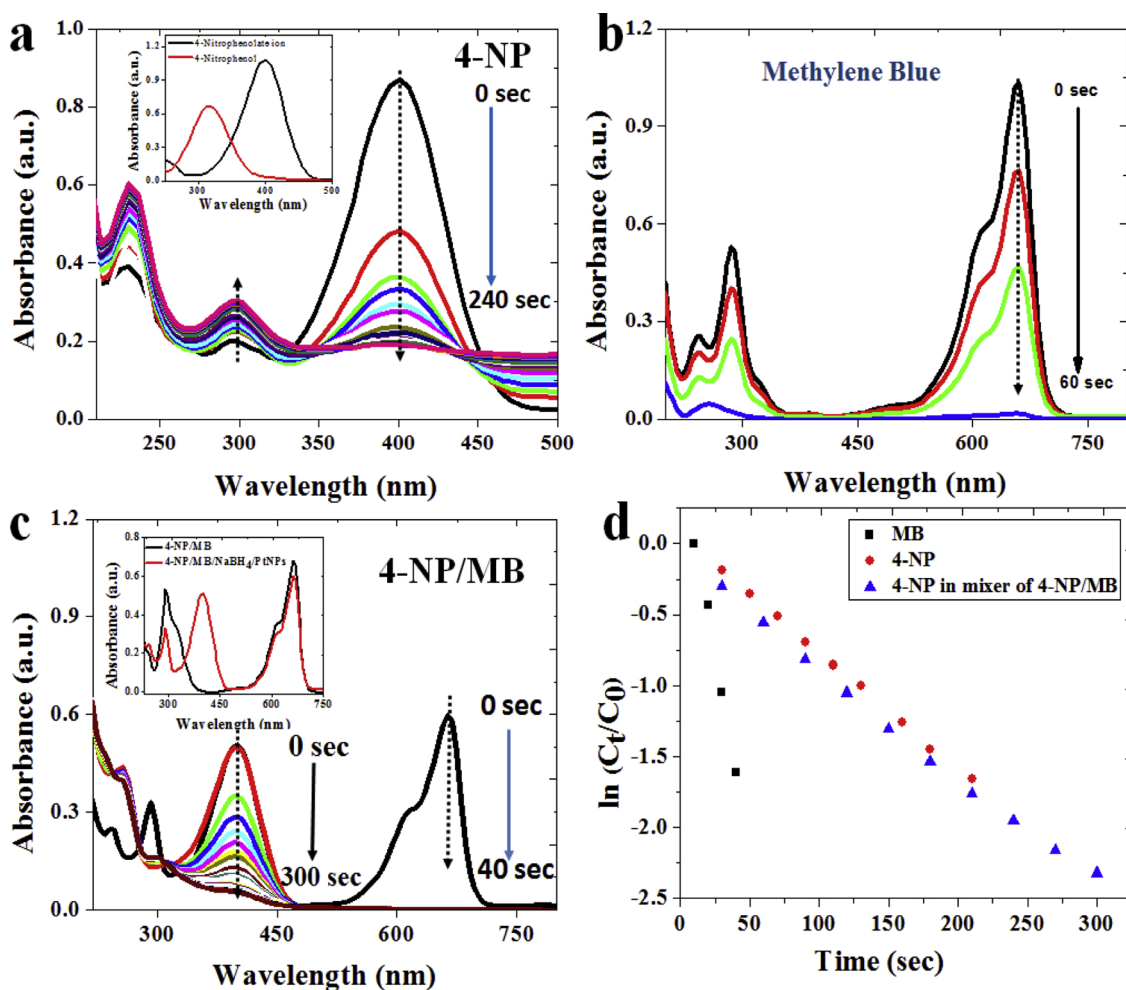


Fig. 4. Absorption spectra of industrial pollutants as a function of time (a) 4-NP, (b) MB, (c) 4-NP + MB mixer and (d) kinetics of 4-NP, MB and 4-NP in 4-NP + MB mixer.

an ideally planar molecule, MB can be readily adsorbed through π - π electron donor acceptor interactions between the aromatic backbone of MB and the carbon from biomass. The high reduction capacity and fast reduction rate of MB and 4-NP over the Pt superstructures probably resulted from the physisorption of organic molecules onto carbonaceous biomass and high reduction ability of the constituent PtNPs. As compared to the other promising catalysts reported in the literature (Table 3), SA-PtNPs reveal 100% reduction of both the organic pollutants in a very short span of time with relatively less amount of catalyst.

Table 1

4-Nitrophenol (4-NP) reduction (to 4-AP) capacity of the fabricated Pt superstructures in comparison with other reported catalysts.

Catalyst	Amount of PtNPs	$C_{\text{NaBH}_4}:C_{4\text{-NP}}$	Reduction time (sec)	Rate constant (sec^{-1})	References
Pt Nano flowers	0.25 mg/ mL	10:1	6000	7.0×10^{-4}	[46]
Pt/meso-CeO ₂	1.0 mg/mL	10:1	480	6.03×10^{-5}	[26]
Pt/nano-CeO ₂			720	4.07×10^{-3}	
C-PtNPs	2.9 mg/mL	42:0.14	3600	5.0×10^{-4}	[27]
P-PtNPs			60	3.0×10^{-2}	
Pt-Fe ₂ O ₃ Micro flowers	5.0 mg/-	100:1	720	0.24 min^{-1}	[47]
Core Shell Ag@Pt NPs sepiolite (Ag:Pt = 1:2)	0.1 g/-	40:0.2	900 (96% reduction)	NR	[48]
PtSnZn nano sheet	(Pt:Sn:Zn = 3.3:2:1) 3.8 $\mu\text{g}/-$	15:0.2	500	4.66×10^{-3}	[49]
SA-PtNPs	0.8 mg/mL	100:1	240	6.0×10^{-2}	Present work

NR = Not reported.

Table 2

Comparison of MB reduction capacity of SA-PtNPs with other reported catalysts.

Catalyst	Reduction capacity (g^{-1})	Reference
Fe ₃ O ₄ @PDA	0.169	[50]
Pt/Rh Nanoparticles	0.347	[51]
Carbon furnished monodisperse Pt nanocomposite	0.196	[29]
SA-PtNPs	39.87	Present work

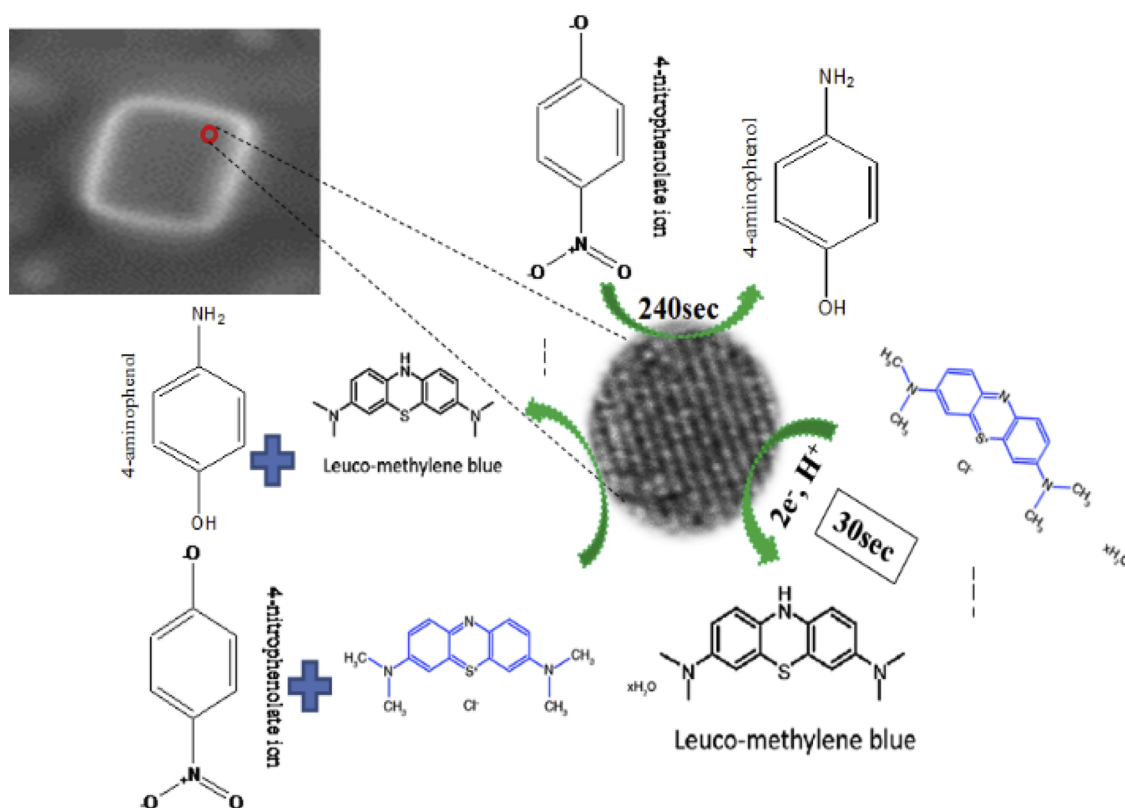


Fig. 5. Schematic presentation of the plausible mechanisms involved in the reduction of industrial pollutants in liquid samples.

Table 3

Comparison of catalytic activity (reduction capacity) of SA-PtNPs with other catalysts for the reduction of mixed pollutants.

Catalyst	Mixed pollutants	Amount of catalyst	% of reduction	Time (min)	Reference
CuFe ₂ O ₄ NPs	MB/MO	8.05 mM	100/10 ± 2	15	[30]
	MB/R6G		100/40 ± 1	18	
	MB/RB		100/50 ± 3	15	
AuNPs embedded into magnetic carbon	MB/MO	8.0 mg/mL	100/10 ± 2	14	[52]
	MB/R6G		100/20 ± 3	14	
	MB/RB		100/7 ± 2	14	
Nanocages	MB/RB		100/7 ± 2	14	
PLDH Composites	RB/CV/MB	50.0 mgL ⁻¹	100/100/100	320	[53]
SA-PtNPs	MB/4-NP	0.8 mgL ⁻¹	100%/100%	5	Present work

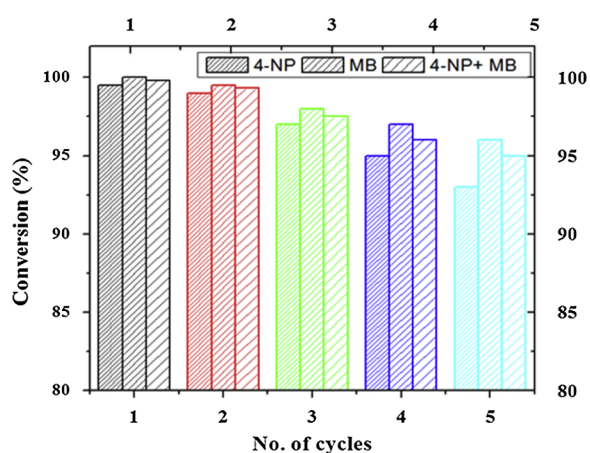


Fig. 6. Reusability of SA-PtNPs for the reduction of 4-NP, MB and 4-NP/MB mixer in the presence of NaBH₄.

3.5. Reusability tests of Pt superstructures in the reduction of 4-NP, MB and 4-NP + MB

The reusability of SA-PtNPs in catalysis was studied by repeated use of the catalyst for several times (Fig. 6). One significant advantage of the assembled particles is their facile recovery simply by centrifugation. The conversion percentage of 4-NP, MB and 4-NP + MB revealed an insignificant decrease of about 2% after 3 cycles, confirming the possible application of SA-PtNPs as an excellent reusable catalyst. This can be attributed to the assembled nature of the particles contributing to the very limited loss during the repeated centrifugation separation process.

3.6. Reduction of industrial organic pollutants adsorbed over silica

In order to test the efficiency of SA-PtNPs in reducing the industrial pollutants adsorbed on solid surfaces [54], silica was taken as a model adsorbent. The 4-NP adsorbed silica sample was prepared by the adsorption through drop casting 4-NP (10⁻³ M; 400 μL) at the surface of silica (0.3 g). About 400 μL of 0.1 M NaBH₄ solution was added to the dry silica sample, followed by the addition of well dispersed SA-PtNPs (8 μg/400 μL). The addition of SA-PtNPs in the mixture revealed a

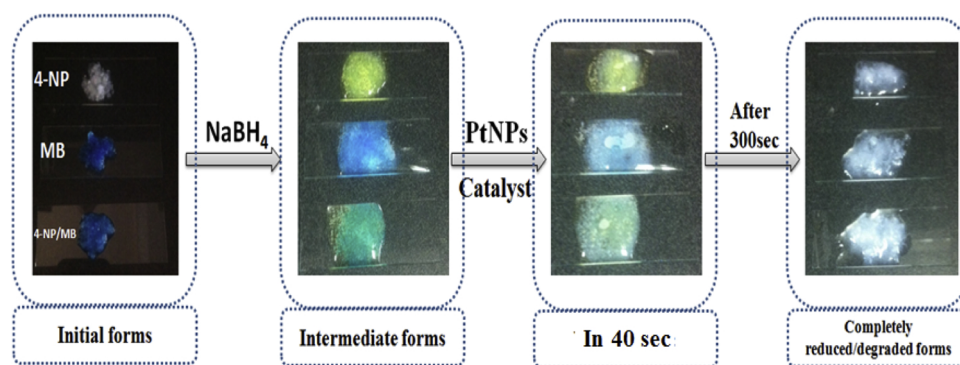


Fig. 7. Photographs showing the different stages of the reduction of industrial pollutants in the adsorbed state (with silica gel as solid adsorbant).

visual color change in silica (from yellow to colorless) in a time span of approximately 240 s. Similar observations were made for the degradation of MB-adsorbed silica (degradation time approx. 40 s). For the mixed pollutant (4-NP + MB) adsorbed on silica, addition of NaBH_4 changed its appearance from blue to green, which eventually turned colorless in approximately 300 s after the addition of SA-PtNPs of similar concentration. The images depicting the color change at different stages of this test have been shown in Fig. 7. The results obtained in these experiments indicate the fabricated Pt superstructures (SA-PtNPs) are equally efficient for the reduction/degradation of organic pollutants adsorbed on solid substrates.

4. Conclusion

A simple, one-pot green synthesis method was developed to synthesize monodispersed Pt nanoparticles, self-assembled into square and rectangular-shaped sub-micrometric superstructures. Synthesis of 2D superstructures was carried out using aqueous CAS extract both as reducing and stabilizing agent, requiring no other solvent, surfactant, or reductor. Presence of carbonaceous materials originating from CAS extract biomass at the surface of Pt superstructures of face-centered cubic phase enhances their organic pollutant adsorption capacity. The fabricated SA-PtNPs demonstrate ultra-fast reduction ability of industrial organic pollutants such as 4-NP and MB, both in aqueous solution as well as in adsorbed state over solid surface. The ultra-fast dye degradation kinetics of the fabricated superstructures is attributed to the presence of biomass and oriented functional groups around the uniformly distributed monodispersed self-assembled Pt nanoparticles at their surfaces. While the SA-PtNPs fabricated by the green synthesis process can be easily separated from the catalytic reaction mixture and reused several times with almost no loss in activity, the technique used for their fabrication can be extended for the development of other metallic superstructures and their assembly over functionalized semiconductor surfaces, for utilization as photo anode in photo-electrochemical processes for solar energy conversion (e.g., artificial photosynthesis).

Acknowledgement

VA acknowledges CONAcYt infrastructure project: INFR-2014-01-226291 for acquiring scanning electron microscope as a central facility.

Appendix A. Supplementary data

Supplementary material related to this article can be found, in the online version, at doi:<https://doi.org/10.1016/j.cattod.2019.06.044>.

References

- [1] Y. Xia, Y. Xiong, B. Lim, S.E. Skrabalak, Shape-controlled synthesis of metal nanocrystals: simple chemistry meets complex physics, *Angew. Chem. Int. Ed.* 48 (2009) 60–103.
- [2] N.L. Rosi, C.A. Mirkin, Nanostructures in biodiagnostics, *Chem. Rev.* 105 (2005) 1547–1562.
- [3] D.K. Gramotnev, S.I. Bozhevolnyi, Plasmonics beyond the diffraction limit, *Nature Photon.* 4 (2010) 83–91.
- [4] C. Burda, X. Chen, R. Narayanan, M.A. El-Sayed, Chemistry and properties of nanocrystals of different shapes, *Chem. Rev.* 105 (2005) 1025–1102.
- [5] A. Kalsin, M. Fialkowski, et al., Electrostatic self-assembly of binary nanoparticle crystals with a diamond-like lattice, *Science* 312 (2006) 420–424.
- [6] D. Zhang, R. Wang, et al., Synthesis of ultra-long copper nanowires for high-performance transparent electrodes, *J. Am. Chem. Soc.* 134 (2012) 14283–14286.
- [7] S. Linic, P. Christopher, D.B. Ingram, Plasmonic-metal nanostructures for efficient conversion of solar to chemical energy, *Nat. Mater.* 10 (2011) 911–921.
- [8] Y. Yin, R.M. Rioux, et al., Formation of hollow nanocrystals through the nanoscale Kirkendall effect, *Science* 304 (2004) 711–714.
- [9] C.N.R. Rao, A. Arulrajdag, A.K. Cheethamdag, B. Raveau, *J. Phys. Condens. Matter* 12 (2010) 7.
- [10] L. Cao, X. Jiao, D.S. Zuzga, Y. Liu, D.M. Fong, D. Young, During, VEGF links hippocampal activity with neurogenesis, learning and memory, *M.J. Nat. Genet.* 36 (2004) 827–835.
- [11] S. Pandey, B.M. Shivani, Catalytic reduction of p-nitrophenol by using platinum nanoparticles stabilised by guar gum, *Carbohydr. Polym.* 113 (2014) 525–531.
- [12] M. Stefanos, A. Thomas, M. Luis, B.B. Sara, P.S. Isabel, Pérez-Justea, Hydrophilic Pt nanoflowers: synthesis, crystallographic analysis and catalytic performance, *J. Cryst. Eng. Comm.* (2016), <https://doi.org/10.1039/C6CE00039H>.
- [13] Q. Wang, Y. Zhang, Y. Zhou, Z. Zhang, J. Xue, Y. Xu, C. Zhang, X. Sheng, N. Kui, Nanocasting synthesis of an ordered mesoporous CeO₂-supported Pt nanocatalyst with enhanced catalytic performance for the reduction of 4-nitrophenol, *RSC Adv.* 6 (2016) 730.
- [14] J.-G. Youa, C. Shanmugama, Y.-W. Liu, C.-Ju. Yu, W.-L. Tseng, Boosting catalytic activity of metal nanoparticles for 4-Nitrophenol reduction: modification of metal nanoparticles with poly(diallyldimethylammonium chloride), *J. Hazard. Mater.* (2016), <https://doi.org/10.1016/j.jhazmat.2016.11.007>.
- [15] P. Zhang, X. Yang, H. Peng, D. Liu, H. Lu, J. Wei, J. Gui, Magnetically recoverable hierarchical Pt/Fe₂O₃ microflower: superior catalytic activity and stability for reduction of 4-nitrophenol, *Catal. Commun.* (2017), <https://doi.org/10.1016/j.cattod.2017.06.047>.
- [16] Y. Maa, X. Wu, G. Zhang, Core-shell Ag@Pt nanoparticles supported on sepiolite nanofibers for the catalytic reduction of nitrophenols in water: Enhanced catalytic performance and DFT study, *Appl. Catal. B: Environ.* (2016) <https://doi.org/doi:10.1016/j.apcatb.2016.12.025>.
- [17] B. Dhandayuthapani, R. Mallampati, D. Sriramulu, R.F. Dsouza, S. Valiyaveetil, PVA/Gluten hybrid nanofibers for removal of nanoparticles from water, *ACS Sustain. Chem. Eng.* 2 (2014) 1014–1021.
- [18] J. Kumar, R. Mallampati, A. Adin, S. Valiyaveetil, Functionalized carbon spheres for extraction of Na-nanoparticles and catalyst support in water, *ACS Sustain. Chem. Eng.* 2 (2014) 2675–2682.
- [19] M. Wu, Y. Li, R. Yue, X. Zhang, Y. Huang, Removal of silver nanoparticles by mussel-inspired Fe₃O₄@ polydopamine core-shell microspheres and its use as efficient catalyst for methylene blue reduction, *Sci. Rep.* 7 (2017) 42773.
- [20] Y. Yunus, O.O. Tugba, I. Betu, G. Bahdisen, K. ultan, S. Aysun, D. Enes, D. Zeynep, S. Hakan, S. Fatih, Highly monodisperse Pt/Rh nanoparticles confined in the graphene oxide for highly efficient and reusable sorbents for methylene blue removal from aqueous solutions, *Chem. Select* 2 (2017) 697–701.
- [21] Chenyu Wang, Carrie Siu, Jun Zhang, Jiye Fang, Understanding the forces acting in self-assembly and the implications for constructing three-dimensional (3D) supercrystals, *Nano Res.* 8 (8) (2015) 2445–2466, <https://doi.org/10.1007/s12274-015->

- 0767-1.
- [22] JoséL. Bott-Neto, Watson Beck, Laudemir C. Varanda, A. Edson, Ticianelli, Electrocatalytic activity of platinum nanoparticles supported on different phases of tungsten carbides for the oxygen reduction reaction, *Int. J. Hydrogen Energy* 42 (32) (2017) 20677–20688, <https://doi.org/10.1016/j.ijhydene.2017.07.065>.
- [23] M.G.ómez-Marín Ana, JoséLuiz Bott-Neto, João B. Souza, Tiago L. Silva, Watson Beck, Laudemir C. Varanda, Edson A. Ticianelli, Electrocatalytic activity of different phases of molybdenum carbide/carbon and platinum–molybdenum carbide/carbon composites toward the oxygen reduction reaction, *ChemElectroChem* 3 (10) (2016) 1570–1579.
- [24] Y. Shin, I.-T. Bae, G.J. Exarhos, Green” approach for self-assembly of platinum nanoparticles into nanowires in aqueous glucose solutions, *Colloids Surf. A: Physicochem. Eng. Asp.* 348 (2009) 191–195.
- [25] M. Stefanos, A. Thomas, M. Luis, B.B. Sara, P.S. Isabel, Pérez-Justea, Hydrophilic Pt nanoflowers: synthesis, crystallographic analysis and catalytic performance, *J. Cryst. Eng. Comm.* (2016), <https://doi.org/10.1039/C6CE00039H>.
- [26] Q. Wang, Y. Zhang, Y. Zhou, Z. Zhang, J. Xue, Y. Xu, C. Zhang, X. Sheng, N. Kui, Nanocasting synthesis of an ordered mesoporous CeO₂-supported Pt nanocatalyst with enhanced catalytic performance for the reduction of 4-nitrophenol, *RSC Adv.* 6 (2016) 730.
- [27] J.-G. Youa, C. Shanmugama, Y.-W. Liu, C. -Ju, Yu, W.-L. Tseng, Boosting catalytic activity of metal nanoparticles for 4-Nitrophenol reduction: modification of metal nanoparticles with poly (diallyldimethylammonium chloride), *J. Hazard. Mater.* (2016), <https://doi.org/10.1016/j.jhazmat.2016.11.007>.
- [28] Y. Yunus, O.O. Tugba, I. Betu, G. Bahdisen, K. ultan, S. Aysun, D. Enes, D. Zeynep, S. Hakan, S. Fatih, Highly monodisperse Pt/Rh Nanoparticles confined in the graphene oxide for highly efficient and reusable sorbents for methylene blue removal from aqueous solutions, *Chem. Select* 2 (2017) 697–701.
- [29] H. Sert, Y. Yildiz, T. Okyay, B. Sen, B. Gezer, S. Bozkurt, G. Başşkaya, F. Sen, Activated carbon furnished monodisperse Pt nanocomposites as a superior adsorbent for methylene blue removal from aqueous solutions, *J. Nano Sci. Nanotechnol.* 17 (2017) 4799–4804.
- [30] L. Wang, G. Hu, Z. Wang, B. Wang, Y. Song, H. Tang, Highly efficient and selective degradation of methylene blue from mixed aqueous solution by using monodisperse CuFe₂O₄ nanoparticles, *RSC Adv.* 5 (2015) 73327.
- [31] Yang Chen, Z. Yao, H.N. Miras, Yu-Fei Song, Modular polyoxometalate-layered double hydroxide composites as efficient oxidative catalysts, *Chem. Eur. J.* 21 (2015) 10812–10820.
- [32] K. Jiahui, B. Christina, S. Varma Rajender, Green synthesis of noble nanometals (Au, Pt, Pd) using glycerol under microwave irradiation conditions, *ACS Sustain. Chem. Eng.* 7 (2013) 810–816.
- [33] K.C. Pratim, L.L. Hsing, G.P. Robert, HSAB principle, *J. Am. Chem. Soc.* 113 (1991) 1855–1856.
- [34] N. Zhang, H. Chuang, Y. Xu, J. Jonathan, Z. Dongtang, C. Jason, K. Stephen, S. Yugang, Near-field dielectric scattering promotes optical absorption by platinum nanoparticles, *Nat. Photo.* 10 (2016) 473–482.
- [35] Y. Xia, Y. Xiong, B. Lim, S.E. Skrabalak, et al., Shape-controlled synthesis of metal nanocrystals: simple chemistry meets complex physics? *Angew. Chem. Int. Ed. Engl.* 48 (2009) 60–103.
- [36] D.R. Vardon, B.K. Sharma, H. Jaramillo, D. Kim, J.K. Choe, P.N. Ciesielski, T.J. Strathmann, Hydro-thermal catalytic processing of saturated and unsaturated fatty acids to hydrocarbons with glycerol for in situ hydrogen production, *Green Chem.* 16 (2014) 1507–1520.
- [37] N.K.R. Bogireddy, H.A.K. Kumar, B.K. Mandal, Reduction of 4-Nitrophenol and production of 4-Aminophenol at ambient conditions by *Sterculia acuminata* fruits extract mediated synthesized platinum nanoparticles, *Mech. Mater. Sci. Eng.* 16 (2018) 1–8.
- [38] Z.Y. Tang, Z.L. Zhang, Y. Wang, S.C. Glotzer, N.A. Kotov, Self-assembly of CdTe nanocrystals into free-floating sheets, *Science* 314 (2006) 274–278.
- [39] K.M. Kumar, B.K. Mandal, S.K. Tammina, Green synthesis of nano platinum using naturally occur-ring polyphenols, *RSC Adv.* 12 (2013) 4033–4039.
- [40] P. Larkin, Infrared and Raman Spectroscopy: Principles and Spectral Interpretation; Waltham, MA, USA, (2011), p. 61 105, 141, 145.
- [41] C. Chunping, G. Poernomo, X. Rong, Self-assembled Fe₃O₄-layered double hydroxide colloidal nanohybrids with excellent performance for treatment of organic dyes in water, *J. Mater. Chem.* 21 (2011) 1218–1225.
- [42] N. Zhihong, P. Alla, K. Eugenia, Properties and emerging applications of self-assembled structures made from inorganic nanoparticles, *Nat. Nano Tech.* 5 (2010) 15–25.
- [43] M.Z. Chaleshtori, V. Correa, N. López, M. Ramos, R. Edaltpour, N. Rondeau, R.R. Chianelli, Synthesis and evaluation of porous semiconductor hexaniobate nanotubes for photolysis of organic dyes in wastewater, *Catalysts* 4 (2014) 346–355.
- [44] N.K.R. Bogireddy, U. Pal, L.-M. Gomez, V. Agarwal, Size controlled green synthesis of gold nanoparticles using Coffea arabica seed extract and their catalytic performance in 4-nitrophenol reduction, *RSC Adv.* 8 (2018) 24819–24826.
- [45] N.K.R. Bogireddy, H.A.K. Kumar, B.K. Mandal, Biofabricated silver nanoparticles as green catalyst in the degradation of different textile dyes, *J. Environ. Chem. Eng.* 4 (2016) 56–64.
- [46] M. Stefanos, A. Thomas, M. Luis, B.B. Sara, P.S. Isabel, Pérez-Justea, Hydrophilic Pt nanoflowers: synthesis, crystallographic analysis and catalytic performance, *J. Cryst. Eng. Comm.* (2016), <https://doi.org/10.1039/C6CE00039H>.
- [47] P. Zhang, X. Yang, H. Peng, D. Liu, H. Lu, J. Wei, Gui, Magnetically recoverable hierarchical Pt/Fe₂O₃ microflower: superior catalytic activity and stability for reduction of 4-nitrophenol, *J. Catal. Commun.* (2017), <https://doi.org/10.1016/j.catcom.2017.06.047>.
- [48] Y. Maa, X. Wua, G. Zhang, Core-shell Ag@Pt nanoparticles supported on sepiolite nanofibers for the catalytic reduction of nitrophenols in water: enhanced catalytic performance and DFT study, *Appl. Catal. B: Environ.* (2016) <https://doi.org/doi:10.1016/j.apcatb.2016.12.025>.
- [49] S.S. Sarmoor, S.J. Hoseini, R.H. Fath, M. Roushani, M. Bahrami, Facile synthesis of PtSnZn nanosheet thin film at oil–water interface by use of organometallic complexes: an efficient catalyst for methanol oxidation and p-nitrophenol reduction reactions, *Appl. Org. Chem.* (2017) e3979, <https://doi.org/10.1002/aoc.3979>.
- [50] M. Wu, Y. Li, R. Yue, X. Zhang, Y. Huang, Removal of silver nanoparticles by mussel-inspired Fe₃O₄@ polydopamine core-shell microspheres and its use as efficient catalyst for methylene blue reduction, *Sci. Rep.* 7 (2017) 42773.
- [51] Y. Yunus, O.O. Tugba, I. Betu, G. Bahdisen, K. ultan, S. Aysun, D. Enes, D. Zeynep, S. Hakan, S. Fatih, Highly monodisperse Pt/Rh nanoparticles confined in the graphene oxide for highly efficient and reusable sorbents for methylene blue removal from aqueous solutions, *Chem. Select* 2 (2017) 697–701.
- [52] W. Zuo, G. Chena, F. Chena, S. Li, B. Wang, Green synthesis and characterization of gold nanoparticles embedded into magnetic carbon nanocages and their highly efficient degradation of methylene blue, *RSC Adv.* 6 (2016) 28774–28780.
- [53] Yang Chen, Z. Yao, H.N. Miras, Yu-Fei Song, Modular polyoxometalate-layered double hydroxide composites as efficient oxidative catalysts, *Chem. Eur. J.* 21 (2015) 10812–10820.
- [54] D. Rambabu, C.P. Pradeep, A. Pooja Dhir, Self-assembled material of palladium nanoparticles and a thiacalix[4]arene Cd(II) complex as an efficient catalyst for nitro-phenol reduction, *New J. Chem.* 39 (2015) 8.